Electronic Supplementary Material (ESI) for Materials Horizons.
This journal is © The Royal Society of Chemistry 2023

Supplementary information

Intensive harmonized synapses with amorphous Cu_2O-based memristors using ultrafine Cu nanoparticle sublayers formed *via* atomically controlled electrochemical pulse deposition

Dong Su Kim,†[a] Hee Won Suh,†[a] Sung Woon Cho,†[b] Shin Young Oh,[a] Hak Hyeon Lee,[a] Kun Woong Lee,[a] Ji Hoon Choi[a] and Hyung Koun Cho[a]*

[a] School of Advanced Materials Science and Engineering, Sungkyunkwan University, 2066, Seobu-ro, Jangan-gu, Suwon-si, Gyeonggi-do 16419, Republic of Korea

[b] Department of Advanced Components and Materials Engineering, Sunchon National University, 255, Jungang-ro, Suncheon-si, Jeollanam-do, Republic of Korea

† The authors contributed equally to this work.

* Corresponding author. Tel.: +82 31 290 7364; Fax: +82 31 290 7410; E-mail: chohk@skku.edu

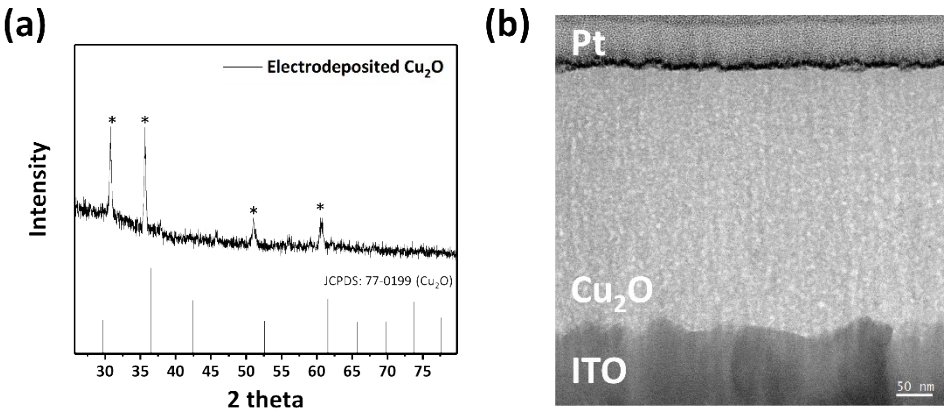

Fig. S1 (a) X-ray diffraction patterns of electrodeposited Cu_2O film. The film is based on an amorphous matrix and has no peaks matching crystalline Cu_2O The four-star marks are patterns of ITO substrate. (b) A transmission electron microscopy (TEM) image of electrodeposited Cu_2O film. No grain boundaries are observed.

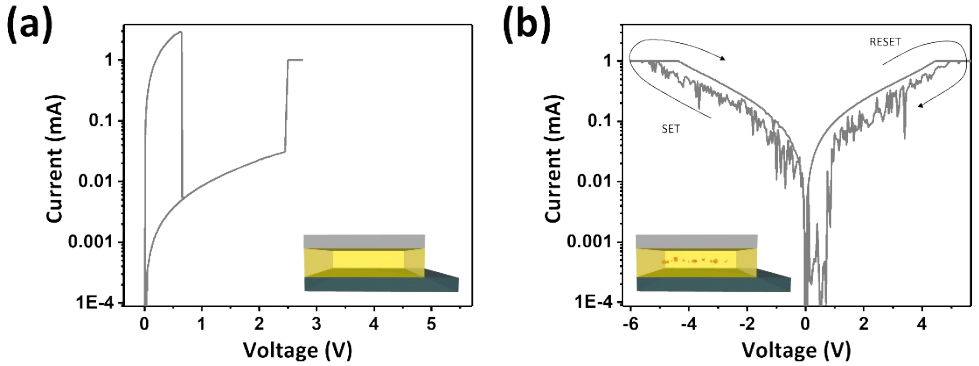

Fig. S2 Representative resistive switching behaviors of (a) ITO/Cu_2O/Pt device and (b) ITO/Cu_2O/Sputtered Cu NPs/Cu_2O/Pt device. (a) exhibits behaviors of unipolar resistive switching and electroforming-free. (b) exhibits a bipolar and noisy resistive switching.

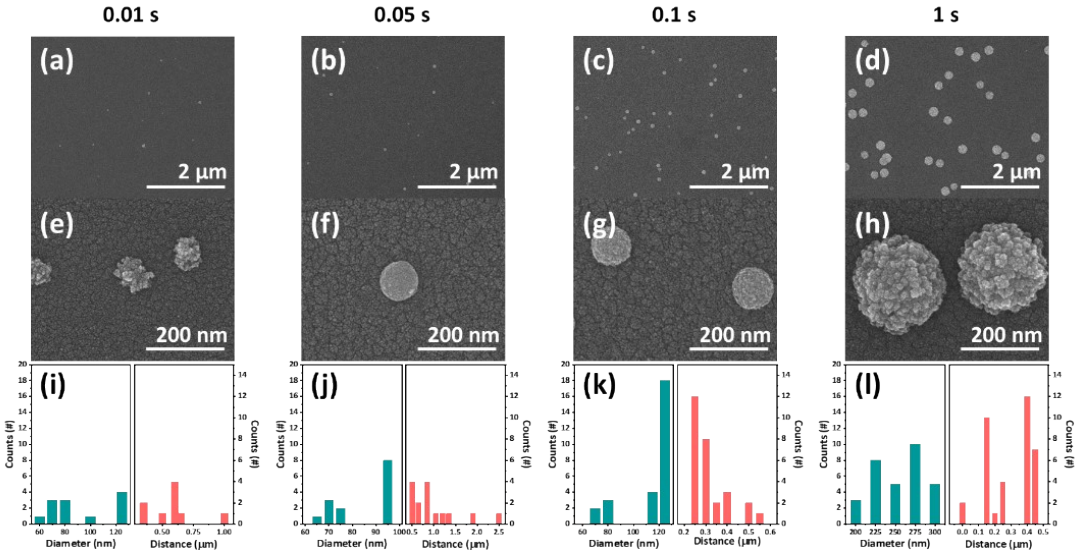

Fig. S3 SEM images showing the time evolution of electrochemically generated Cu nanoparticles on ITO substrates.

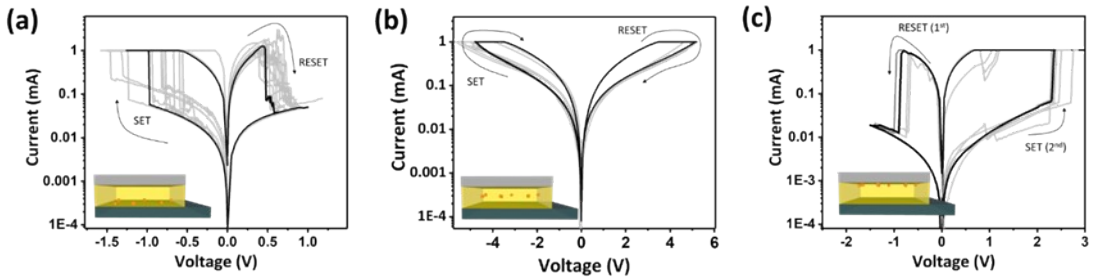

Fig. S4 1st, 10th, 20th … 100th RS cycles under the IV-sweep mode for the device of (a) BU-Cu NPs, (b) CU-Cu NPs, and (c) TU-Cu NPs. The compliance current (I_{CC}) was set 1 mA.

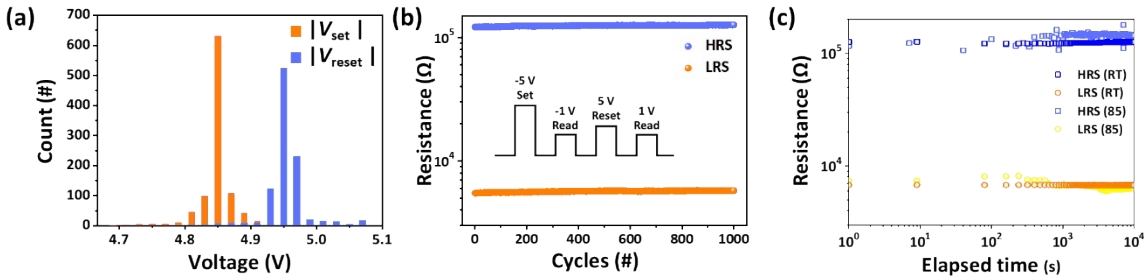

Fig. S5 Electrical performances of the ITO/Cu_2O/U-Cu NPs/Cu_2O/Pt RRAM device: (a) The set/reset voltage distribution of 1000 repeated RS cycles. (b) Endurance test of HRS/LRS distribution of 1000 cycles at RT. (c) Retention test of HRS/LRS for 10^4 s at RT and 85 °C.

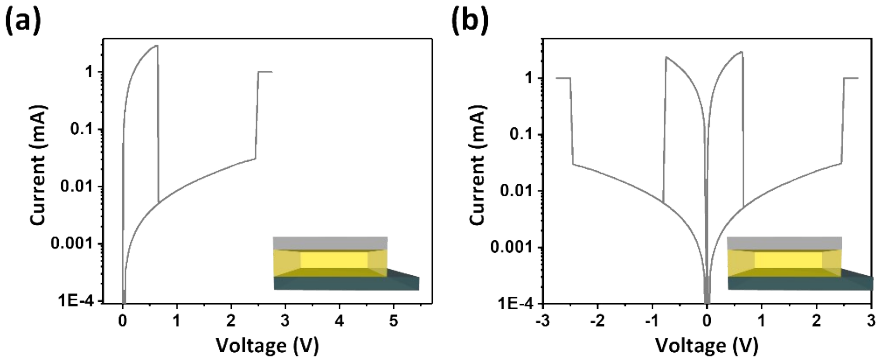

Fig. S6 The unipolar set-reset characterization of pristine ITO/Cu_2O/Pt device in (a) only positive sweep and (b) both positive and negative sweep.

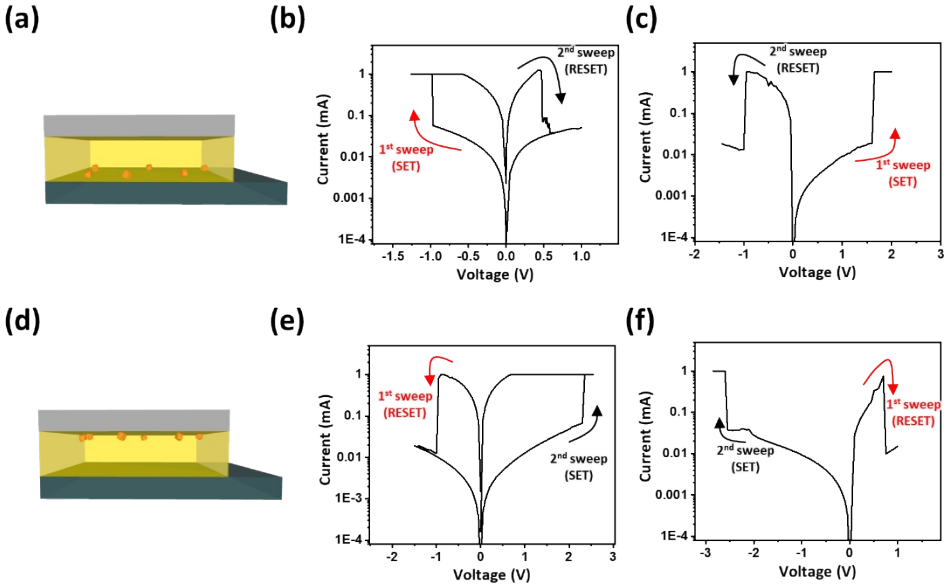

Fig. S7 (a) The schematic structure of BU-Cu NPs. The set-reset behavior of BU-Cu NPs with (b) negative set-positive reset and (c) positive set-negative reset. (d) The schematic structure of TU-Cu NPs. The set-reset behaviors of TU-Cu NPs with (e) negative reset-positive set and (f) positive reset-negative set.

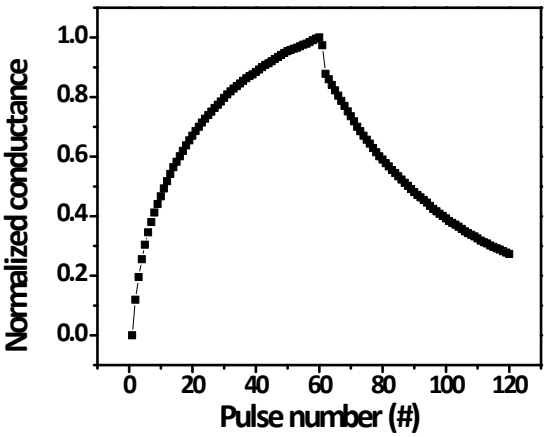

Fig. S8 LTP and LTD updates pristine Cu_2O RRAM device.

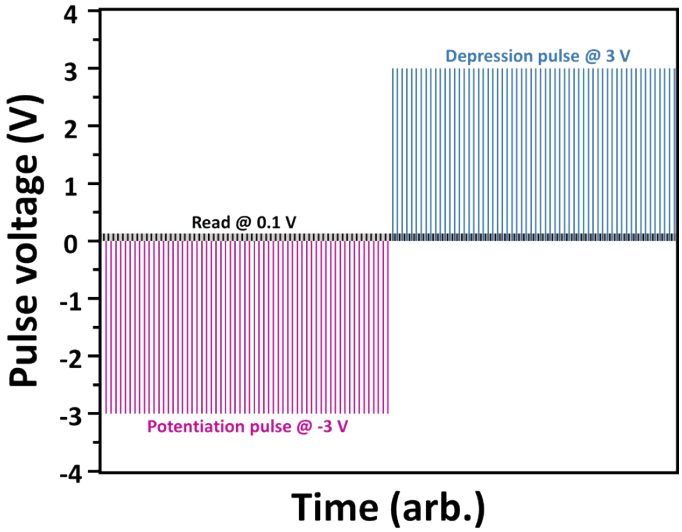

Fig. S9 The employed pulse trains to test synaptic plasticity. The potentiation pulse and the depression pulse were applied after the read pulse, respectively, and a total of 60 potentiation pulses and 60 depression pulses were used. The pulse width and interval were set to 10 μs and 50 μs, respectively.

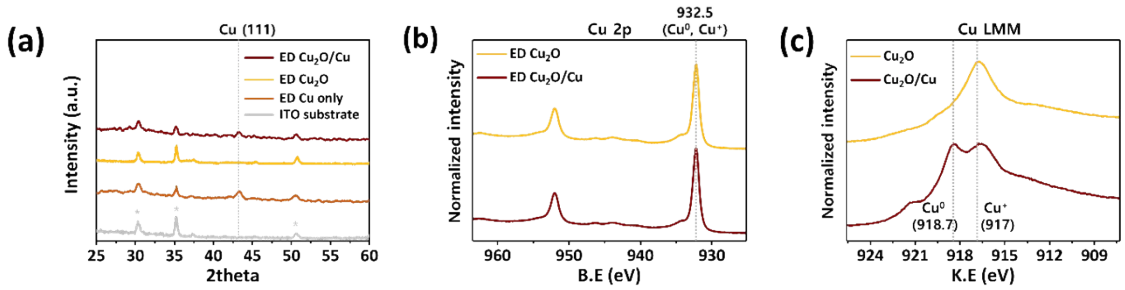

Fig. S10 (a) XRD analysis of the electrodeposited Cu_2O/Cu, Cu_2O, and Cu films together with ITO reference: Cu_2O (yellow line, ED @ -0.4 V vs vs. Ag/AgCl) and Cu film (orange line, ED @ -1 V vs vs. Ag/AgCl). (b) and (c) XPS and AES analysis of electrodeposited Cu_2O film (yellow line) and Cu_2O film with Cu nanoparticles (brown line).

First, to analyze the presence and phase of the formed Cu-based phase at –0.45 V or –1 V vs. Ag/AgCl, XRD analysis of the thin film deposited with an intentionally high thickness (300 nm) was additionally performed (Fig. S10a). In the XRD data, specific ED Cu_2O peaks were not observed for the embedded nanoparticles in the amorphous matrix (yellow line). However, the ED Cu metal with strong crystallinity was confirmed to have a (111) peak at 43.3°, which was also produced on Cu_2O by the additional pulse deposition method (red line).

Second, the XPS is one of the best methods for investigating the chemical composition and electronic structure of surface transformations. Through XPS analysis, as shown in **Figs. S10b and 1c**, the surfaces of Cu_2O deposited at –0.4 V and pulse electrodeposited Cu_2O/Cu were compared. The main peaks of Cu 2p3/2 consisted of Cu^0 at 932.61 eV, Cu^+ at 932.28 eV and Cu^{2+} at 934.7 ± 0.1 eV. For both the ED Cu_2O and ED Cu_2O/Cu, only a single peak at 932.5 eV was observed, and no additional satellite peaks related to Cu^{2+} (CuO phase) were observed. However, the peak at 932.5 eV can be assigned to either Cu^+ or Cu^0 because their binding energies almost overlap in the spectrum of Cu 2p3/2.

To further confirm this contribution, we examined the CuL3M4.5M4.5 Auger peaks, from which the modified Auger parameter was calculated (**Fig. S10c**). This parameter also allowed us to distinguish between Cu^+ and Cu^0, which show almost the same chemical shift as Cu2p. Based on the pristine Cu_2O peak, Cu_2O/Cu had an additional shoulder at 918.7 eV, originating from Cu. The distinct separation of the two shoulders indicates that Cu_2O and Cu were simultaneously exposed on the surface of the active layer.

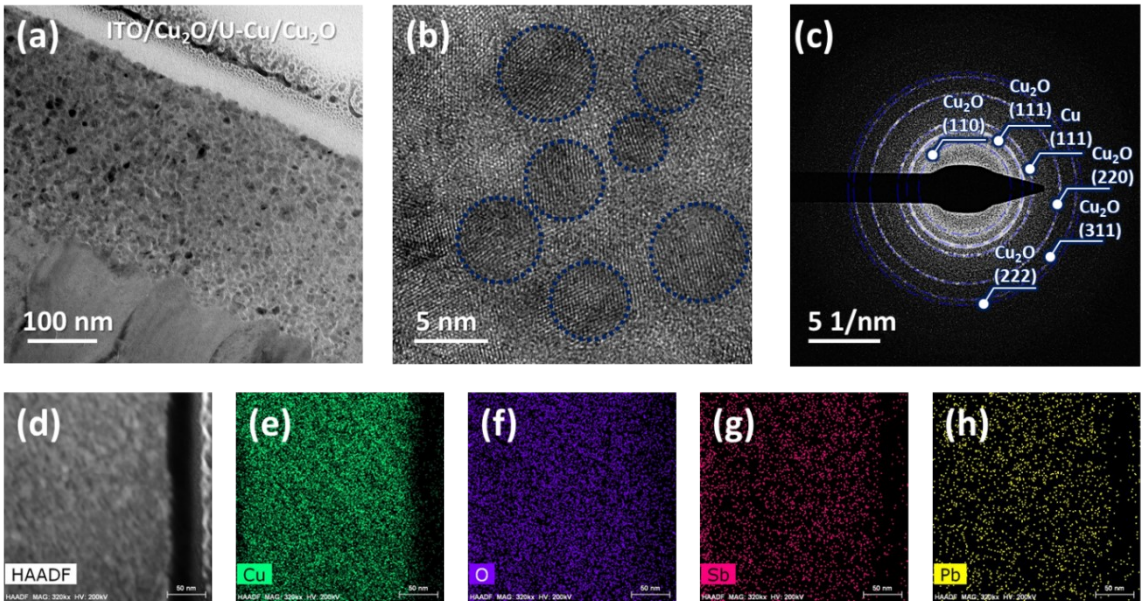

Fig. S11 (a) The low magnified and (b) high magnified HRTEM images. (c) SAED pattern of Cu_2O active layer. (d) The HAADF-STEM image of Cu_2O active layer and elemental mapping for (e) Cu, (f) O, (g) Sb, and (h) Pb elements.

Third, the pulse-deposited Cu_2O active layer with nanoparticles embedded in an amorphous matrix was confirmed through the TEM image and energy-dispersive X-ray (EDX) analysis, as shown in **Fig. S11**. A SAED pattern of pulse deposited Cu_2O active layer (**Fig. S11c**) revealed six sets of rings, indicating the coexistence of Cu and Cu_2O phases. In addition, the Sb and Pb dopants were evenly dispersed, leading to an amorphous growth (**Figs. 11d–h**).

To clearly observe the Cu NPs, HR-TEM analysis was performed with ITO/Cu_2O/U-Cu. The Cu NPs obtained from the electrochemical deposition were uniformly generated on the surface (**Fig. S12**).

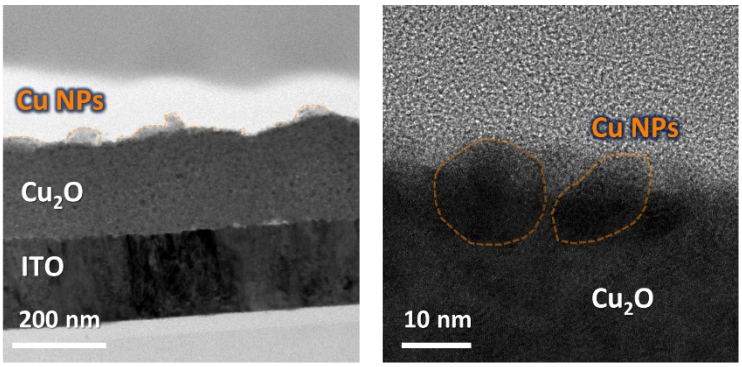

Fig. S12 HRTEM image of ITO/Cu_2O/U-Cu NPs.

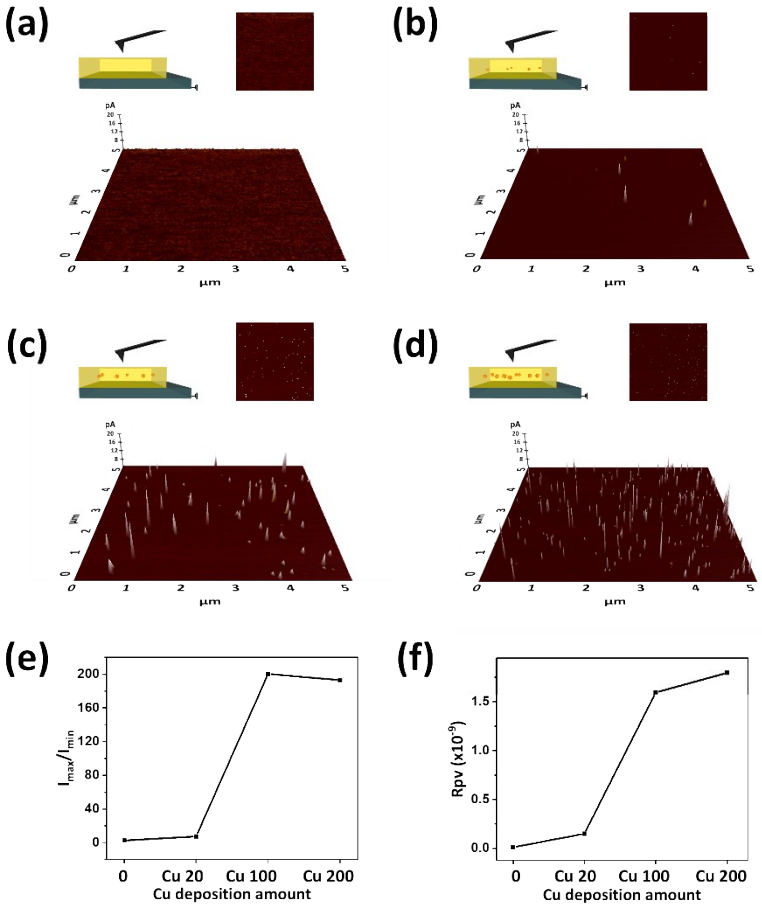

Fig. S13. Conductive atomic force microscope (C-AFM) analyses of ITO/Cu_2O/U-Cu NPs/Cu_2O/Pt devices in HRS state. The local current images from (a) pristine Cu_2O device, (b) U-Cu 20 device, (c) U-Cu 100 device, and (d) U-Cu 200 device. (e) The ratio of maximum current to minimum current. The values are 2.55, 7.66, 200.25, and 192.85. (d) The peak-to-valley of the selected region (R_{pv}), which represents the difference in I_{max} and I_{min}, had values of 9.203E-12A, 1.49E-10A, 1.595E-9A, and 1.795E-9A. The Cu 100 device and the Cu 200 device have candidate sites that can concentrate the injected electric field.

Table S1 Performance comparison.

Structure	Active layer	Switching type	Set voltage (V)	Reset voltage (V)	Endurance (Cycle)	Retention (Time)	Nonlinearity (%) (LTP/LTD)	Accuracy (%)	Ref.
ITO/Cu_2O /U-Cu/Cu_2O Pt	Cu_2O	Bi-polar	-3	+3	2000	10^4 s	2.43/0.13	**85.17**	This work
Ta /ZnSnO/TiN	ZnSnO	Bi-polar	-1	1.5	2000	10^4 s	35.51/22.21	45	1
Pt/a-Ta_2O_5/TiN	Ta_2O_5	Bi-polar	-2.4	1.3	100	10^4 s		85	2
Pt/$HfAlO_x$ /TiN	$HfAlO_x$	Bi-polar	-0.8	1	200	10^4 s	211.9/89.12	44.9	3
Al/HfO_2/ Ti/TiN	HfO_2	Bi-polar	2	-1.5	240	10^2 s	16.53/0.99	10	4
Pt/Li_2TiO_3 /Pt	LTO	Bi-polar	-2	2	2000	10^5 s	5.25/1.45	83	5
Pt/AlN/WN/Cu	AlN	Bi-polar	0.7 V	-0.4 V	500	10^4 s	2.3 / 3.5		6
ITO/Al:HfO_x/HfO_x/ Al	HfO_x	Bi-polar	1.4 V	-2.4 V		10^4 s	8.9 / 5.6		7

References

1. Journal of Alloys and Compounds, 2021, 862, 158416

2. Journal of Alloys and Compounds, 2021, 877, 160204

3. RSC Adv., 2020, 10, 31342–31347

4. IEEE Electron Device Letters, 2016, 37, 8, 994

5. ACS Appl. Mater. Interfaces 2022, 14, 4, 5673–5681

6. Electronics 2022, 11(21), 3432

7. IEEE Transactions on electron devices 2022, 69, 1842-1848